Polymer 49 (2008) 3993–3999

Contents lists available at ScienceDirect

Polymer

journal homepage: www.elsevier.com/locate/polymer

Size effect on mechanical properties of micron-sized PS–DVB polymer particles

J.Y. He [a], Z.L. Zhang [a,*], M. Midttun [a], G. Fonnum [b], G.I. Modahl [b], H. Kristiansen [c], K. Redford [c]

[a] NTNU Nanomechanical Laboratory, Norwegian University of Science and Technology, 7049 Trondheim, Norway
[b] Invitrogen Dynal AS, P.O. Box 114, Smestad, 0309 Oslo, Norway
[c] Conpart AS, 2013 Kjeller, Norway

ARTICLE INFO

Article history:
Received 13 February 2008
Received in revised form 30 April 2008
Accepted 7 July 2008
Available online 17 July 2008

Keywords:
PS–DVB particles
Flat punch indentation
Size effect

ABSTRACT

A nanoindentation-based flat punch method has been developed to determine the stress–strain behaviour of single micron-sized Ugelstad polystyrene-*co*-divinylbenzene (PS–DVB) particles in compression. Five groups of particles with identical chemical compositions but different diameters have been tested. The diameter of the PS–DVB particles varied from 2.6 μm to 25.1 μm. Constant relative deformation rate has been applied with two maximum strain levels of 5% and 10%. Results show that the particle compressive stress–strain behaviour is strongly size-dependent. The smaller the particle size is, the stiffer the particle behaves. Analyses indicate that the pre-load and adhesion during the flat punch test play a minor role on the size effect. The presence of a core–shell structure can possibly be a main contribution to the size effect. Finite element analyses have been carried out to demonstrate this surface shell effect.

1. Introduction

Nanoindentation is now a well-established tool for probing the mechanical properties, for example, Young's modulus and hardness, at the micro- and nano-scales [1]. During the indentation, the indentation load and displacement are simultaneously monitored and load–displacement curves are recorded. The material hardness and reduced modulus can be calculated from the contact area determined by the contact depth using an area function of the indentation tip and the contact stiffness obtained by fitting the initial portion of the unloading curve.

One interesting phenomenon, namely indentation size effect (ISE) was revealed more than 50 years ago [2] but so far the mechanisms involved are not fully understood. The hardness defined as the ratio of the applied force to the contact area, is commonly assumed to be independent of the measurement scale. But the hardness measured by nanoindentation for certain metals has been shown to increase with decreasing depth of indentation size within a range typically less than 10 μm [3]. In fact, every metal has an intrinsic material length scale, and for indentation depth less than this, the ISE occurs.

The strain gradient effect [4–6], surface effect [7], non-uniformly deformed microstructure [3], interaction between the indenter and the sample [8] are the possible mechanisms for the ISE. The various mechanisms imply a complicated nature of the ISE. During the last decade, the theory of strain gradient plasticity (SGP) developed by Nix and Gao [4] has received attention. In a nanoindentation test, plastic deformation is confined within a small volume, which results in a strain gradient. According to Taylor's dislocation hardening theory, the stored dislocations, which are caused by a homogeneous strain, and the so-called geometrically necessary dislocations, which are significantly affected by the strain gradient, both contribute to the hardness [9].

Most of the studies on the ISE focused on single crystals and polycrystals. This study will report a new area of the indentation related size effect, related to mechanical deformation of monodisperse polymer particles with low crosslinking density. The particles are synthesized by the Ugelstad method [10], which is a well-known and versatile technology for the manufacturing of monosized polymer particles by a multi-step swelling process. A large number of monomers can be used, and in this case a combination of styrene and DVB has been used giving a crosslinking density of about 2%. The coefficient of variance (C.V.) of the size distribution is less than 2%, in which C.V. is the scatter of probability distribution and is defined by the ratio of the standard deviation to the mean.

Micron-sized polymer particles, of 0.5–100 μm in diameter, are widely used in food, chemical industries and biotechnology. Recently there is a growing interest in extending the polymer particle technology also for microsystem applications by producing nanostructured polymer particles, especially in Anisotropic Conductive Adhesive (ACA) [11–15]. As a substitute for compact metal particles, the polymer core particles increase the compliance of the interconnection and hence improve the reliability. The

* Corresponding author. Tel.: +47 735 92530; fax: +47 735 94701.
E-mail address: zhiliang.zhang@ntnu.no (Z.L. Zhang).

0032-3861/$ – see front matter © 2008 Elsevier Ltd. All rights reserved.
doi:10.1016/j.polymer.2008.07.015

introduction of ACA technology can also contribute with reduced package size, lower assembly temperature, and possibly lower cost. For lager particles used for Ball Grid Arrays (BGA) and Chip Scale Packaging (CSP) there is also a significant advantage in terms of reduced environmental impact [16–19]. The functional performance in these applications is strongly connected to the contact area, which is coupled to the deformation level. Therefore, the mechanical properties of polymer particles are of crucial importance. However, mechanical characterization of single micron-sized particles possesses great challenges, due to the inherent complexity of the spherical geometry and the large deformation involved.

Polymer particles have been used to reinforce the bulk properties of composite materials. The effect of particle size on the bulk mechanical properties of concrete [20], high-impact polystyrene [21–23], polymer blends [24,25] and polymer latex [26] has been studied extensively. Recently, the mechanical properties of bulk polymer materials reinforced with polystyrene and poly(butyl acrylate) core/shell particles with sizes in tens of nanometers have been reported [27]. The mechanical behaviour of the bulk polymer was found to be strongly influenced by the particle size and the distribution of the composing polymers.

In the present study, the effect of the particle size on the mechanical properties of single particles has been studied. Five groups of commercially available polystyrene-*co*-divinylbenzene (PS–DVB) particles (Dynospheres®, Invitrogen Dynal AS, NO) with identical chemical compositions but different diameters have been tested using a nanoindentation-based flat punch method. The particles have the same synthesis procedures and chemical compositions but different diameters. The diameter varied from 2.6 μm to 25.1 μm. The nominal compressive stress–strain behaviours of particles are obtained from nanoindentation-based flat punch test results. The effect of the particle diameter on the compressive stress–strain behaviour is analyzed experimentally and the nature of the particle size effect is discussed.

2. Experiment

2.1. Materials

The five groups of polymer particles are made of the same chemical compositions: 98% polystyrene crosslinked with 2% divinylbenzene by Ugelstad method. The diameters of the particles are 2.6 μm, 5.1 μm, 15.3 μm, 20 μm and 25.1 μm. The C.V.s of the size distribution are 1.7%, 0.8%, 1.2%, 1.6% and 1.0%, respectively. The SEM photographs of the smallest and largest particles are shown in Fig. 1. The dry particles are dispersed in 95% industrial ethanol. The very diluted dispersion is exposed to a high frequency ultrasonic vibration to redisperse the particle clusters. A drop of the ethanol–particle suspension is placed on a bare silicon chip ($10 \times 10 \times 0.5$ mm). The specimens are then conditioned in a clean environment for a specific period of time to remove any ethanol left in the particle.

2.2. Apparatus

The indentation tests are performed using a nanomechanical testing system (TriboIndenter® Hysitron Inc., MN., USA) which has a standard mode and a multi-range mode. The standard mode can reach a maximum load capacity of 10 mN and a maximum indentation depth of 5 μm with a load and displacement resolution of 1 nN and 0.1 nm, respectively. The multi-range mode has a maximum load of 4 N and a maximum indentation depth of 80 μm with a load and displacement resolution of 500 nN and 2 nm. For the polymer particles in this study, a diamond flat punch with 100 μm in diameter was used.

The flat punch is cleaned to remove external impurities such as dust before testing. The flat punch in this experiment requires precise calibration, especially flat punch planarity. The planarity calibration is evaluated by the indents produced by penetration into a polished indium surface. A clean, 100 μm diameter circle impressions well pressed on the surface of the polished indium are required for a flat punch to be acceptable. The relatively tip-optics position is also accurately calibrated through the indents on the polished indium.

2.3. Method

Using the optical microscope, single particle with a sufficient distance (>75 μm) to its closest neighbour is located and used for the indentation tests. Fig. 2 illustrates the contact between a rigid flat punch and a single PS–DVB particle. All indentation tests are performed in air and at room temperature (23 °C). The room humidity is kept constant about 30% through an air ventilation system. The displacement controlled mode which operates the indentation depth versus time is selected in order to control the nominal strain rate for each group of particles. Two deformation levels, 5% and 10% with corresponding nominal strain rates of 0.01/s and 0.02/s with reference to particle diameter, have been applied to all the particles. A typical test is completed in 12 s where the testing displacement function consists of a linear displacement-increasing segment for 5 s, a 2 s displacement-holding segment, and linear displacement-decreasing segment for 5 s. The heat drift of displacement is monitored for 40 s at pre-load 1 μN, and the drift rate calculated by fitting a straight line to the drift displacement versus time graph during the latter 20 s is used to correct the resulting data. For every group of particles, at least three individual

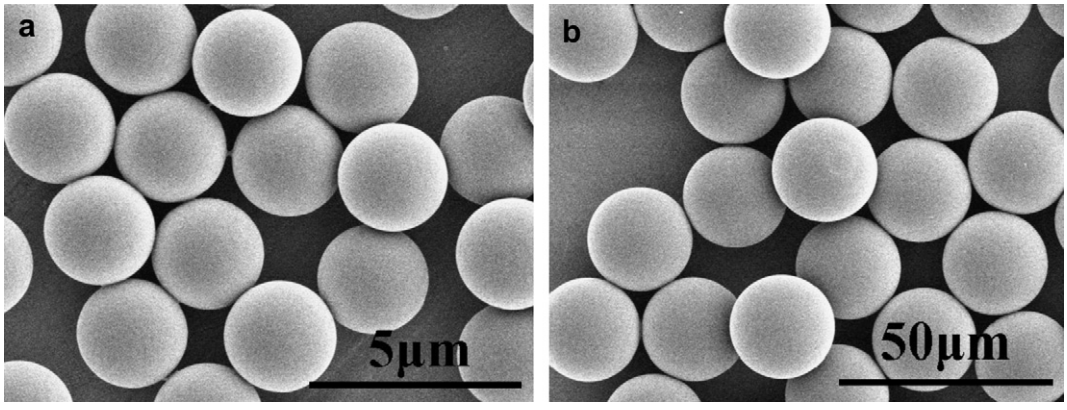

Fig. 1. SEM photographs of (a) the smallest particle and (b) the largest particle.

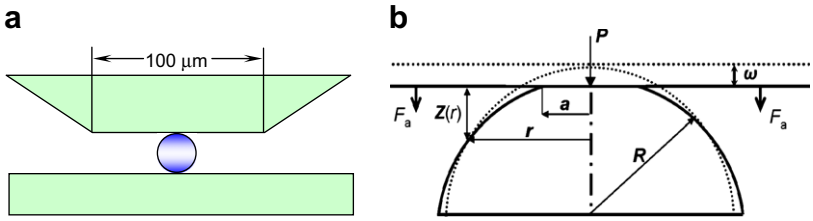

Fig. 2. Schematic plot of the flat punch test (a) and model description (b).

particles are tested in order to check uniformity of particle properties and the repeatability of the results.

Both the standard mode and the multi-range mode are applied. The standard mode is used for testing all the particles up to 5% deformation. For the 10% deformation, multi-range loading mode must be used on the two largest groups of particles. Since two loading modes are involved, it is essential to calibrate the system such that both the standard mode and the multi-range mode yield identical results. The typical indentation force-depth results from the two loading modes with a deformation up to 20% for the 15.3 μm diameter particles are shown in Fig. 3. The results are well matched; however, the curve obtained by the multi-range mode is less smooth due to its inferior feedback system compared with the standard mode. Fig. 3 indicates that it is reasonable to believe that the both loading modes give the same results.

3. Results

Load–displacement curves are obtained for all PS–DVB particles at two deformation levels, 5% and 10% deformation are shown in Fig. 4(a) and (b), respectively. In Fig. 4(a), every group of particles is compressed to a maximum of 5% deformation and represented by four indentation curves. In Fig. 4(b), each group has three indentation curves and is loaded to a maximum of 10% deformation. The loading segments of each group of particles at the same deformation level are found to be quite repeatable and consistent. This is in contrast to typical bulk polymer materials where mechanical properties show a significant scatter due to variations in microstructure, anisotropy, molecular weight, crosslink density, etc. [28]. Thus, the highly consistent load–displacement curves demonstrated for every group of the PS–DVB particles indicate a very homogeneous material including size distribution, microstructure, chemistry and molecular weight. At the same time it also gives confidence to the experimental setup and reproducibility. To reach 10% deformation the two bigger particles have to be tested using the multi-range mode, and the curves are slightly bumpy, but the trends are very similar to those using the standard mode.

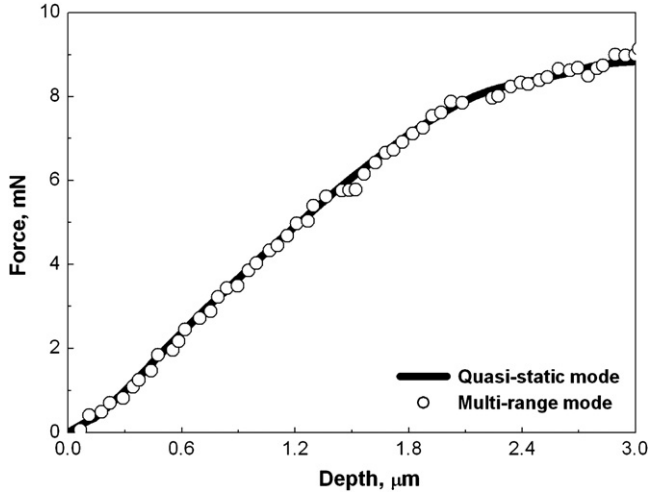

Fig. 3. The loading curves of the 15.3 μm diameter particles with different load modes.

During the large deformation compression, the volume and Poisson's ratio of the polymer particles may change continuously with the deformation because of the spherical geometry. It is not possible to obtain the true stress–strain behaviour of particles from those conditions. To compare the mechanical properties of particles with different sizes, the nominal compressive stress–strain behaviours have been used. These are obtained by normalizing the force to the initial cross-section area and the displacement to the initial diameter of particles [29]:

$$\sigma_c = \frac{P}{\pi R^2} \tag{1}$$

$$\varepsilon_c = \frac{2\omega}{D} = \frac{\omega}{R} \tag{2}$$

where σ_c is the nominal compressive stress, ε_c is the nominal compressive strain, P is the contact load, D is particle diameter, R is the initial particle radius, and ω is the half deformation of the sphere (Fig. 2(b)). The nominal compressive stress–strain curves of the five groups of particles at two deformation levels are displayed in Fig. 5(a) and (b), respectively. The focus of this study is the loading part and the unloading stress–strain curves are omitted in Fig. 5.

From the continuum mechanics point of view, stress–strain behaviour is one of the constitutive properties of materials. For particles with different sizes but same chemistry and same strain rate, all the stress–strain curves should collapse into one. But Fig. 5 clearly shows that the compressive stress–strain behaviours of particles are strongly size-dependent, the smaller the particle size, the harder the particles. The smallest particle is the hardest while the biggest particle is the softest. With the increase of particle size, the size dependence of compressive stress–strain behaviour diminishes gradually.

The nominal compressive stress of all the five groups of particles at 4% deformation level with strain rates 0.01/s and 0.02/s is plotted in Fig. 6, in which the compressive stress is normalized by the corresponding value of the smallest particle. Particles display distinct size effect at both stain rates. The compressive stress of the biggest particle is almost 50% lower than that of the smallest particle at a strain rate of 0.01/s. As the strain rate increases to 0.02/s, the size effect becomes even more pronounced. The size effect also seems to have different trends depending on the strain rate. With the smaller strain rate, the size effect is most evident for the two smaller particle sizes, whereas for the larger strain rate the size effect is more evenly distributed.

4. Discussion

The existing theories for indentation size effect are mainly based on dislocation movement and cannot predict the behaviour

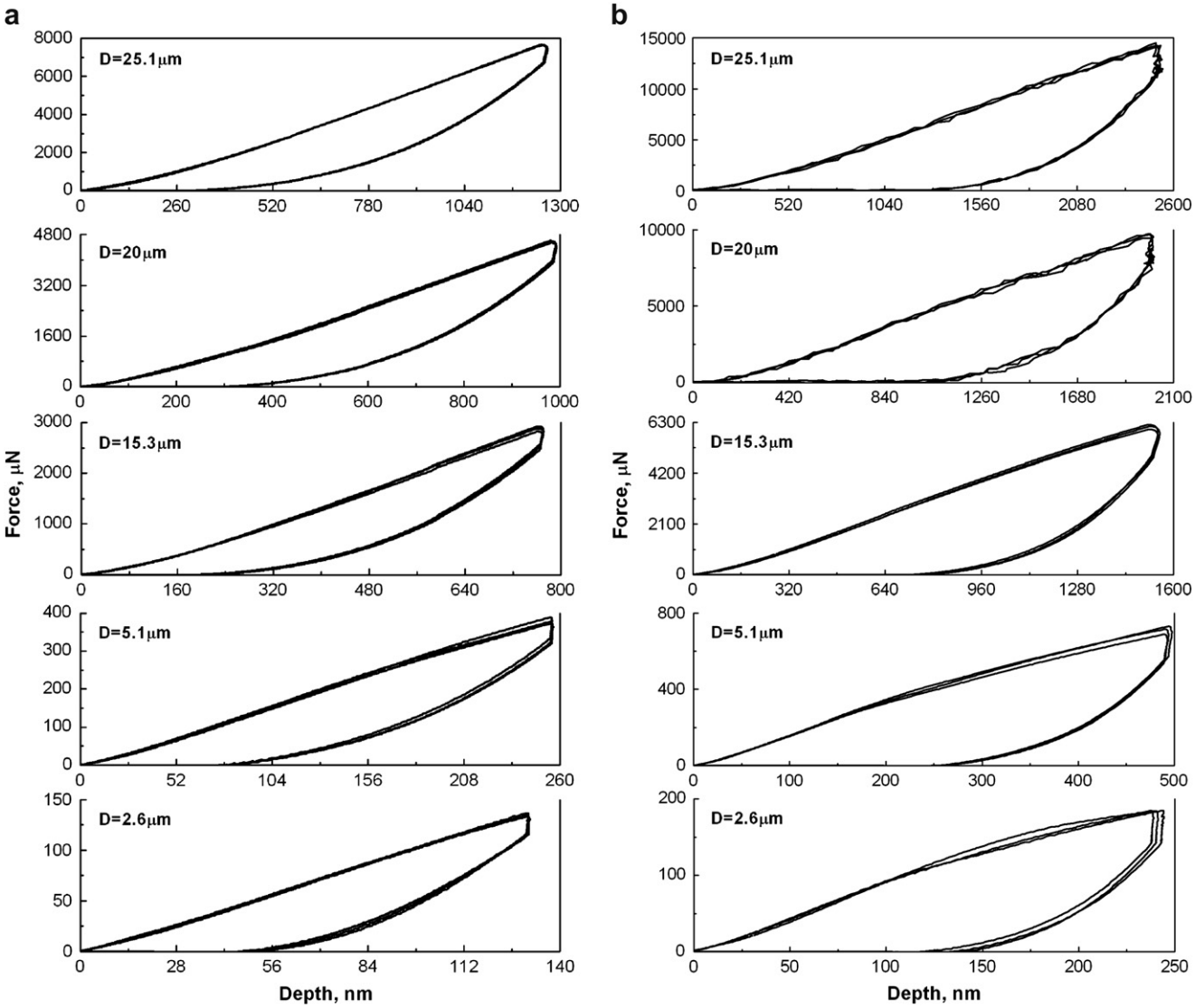

Fig. 4. Indentation load–displacement curves of five group particles (a) at 5% deformation with 0.01/s strain rate and (b) at 10% deformation with 0.02/s strain rate.

observed for the polymer particles. The deformation mechanisms in polymers are very different from metals due to the absence of dislocations. There are three types of solid polymer behaviours [30]: brittle fracture behaviour, yield behaviour and rubber-like behaviour. Brittle fracture behaviour is characterized by no apparent yield point and obeys Hooke's law at low strain level. Yield behaviour exhibits a maximum point followed by strain softening, usually associated with crazing or shear banding which leads to ductile fracture. Rubber-like behaviour is characterized by a plateau in the stress–strain curve. Polystyrene as linear (non-crosslinked) polymer is known to exhibit brittle fracture causing crazing under tensile stress, however, the same material shows yield behaviour displaying shear banding in compression. Crazing deformation is a localized yielding behaviour and can be observed as a whitening of the polymer in the region of maximum deformation. The volume of the polymer increases through formation of micro-cracks, which are bridged by polymer fibrils. Shear banding deformation which is highly dependent on temperature and strain rate is characterized by planes of slip at 45° to the direction of stress and involves the local orientation of the polymer. In contrast, PS–DVB has the microstructure of the crosslinked network, which deforms by the slip of flexible chain. The crosslinking is important to avoid the inter-chain slip. The crosslink density should not only be in a certain range to keep away from the inter-chain slip but also have an enough space between two crosslink points to allow a good deformability.

For the PS–DVB particles there are possibly many factors contributing to the size effect. The experimental method itself may bring some uncertainties to the results. For instance, the pre-load used for determining the zero contact surfaces on the nano-indentation sample is applied to the particles before indentation. Given that the particles do not fully recover after this pre-load, the indentation does therefore not begin from a perfect point contact but with a finite contact area, which will have significant influence at small deformations. Similarly, the adhesion between the soft polymer particle and the rigid flat punch or the substrate could pose a similar effect. During synthesis of PS–DVB particles from water suspension there has been observed a "core–shell" structure [31] on the particles by TEM. In the shell, the crosslink density is much higher than that in the inner particle. This surface shell effect might be prominent for smaller particles.

In the following, potential factors both in the particle synthesis and in the experiments are analyzed in order to clarify the mechanisms of the observed size effect.

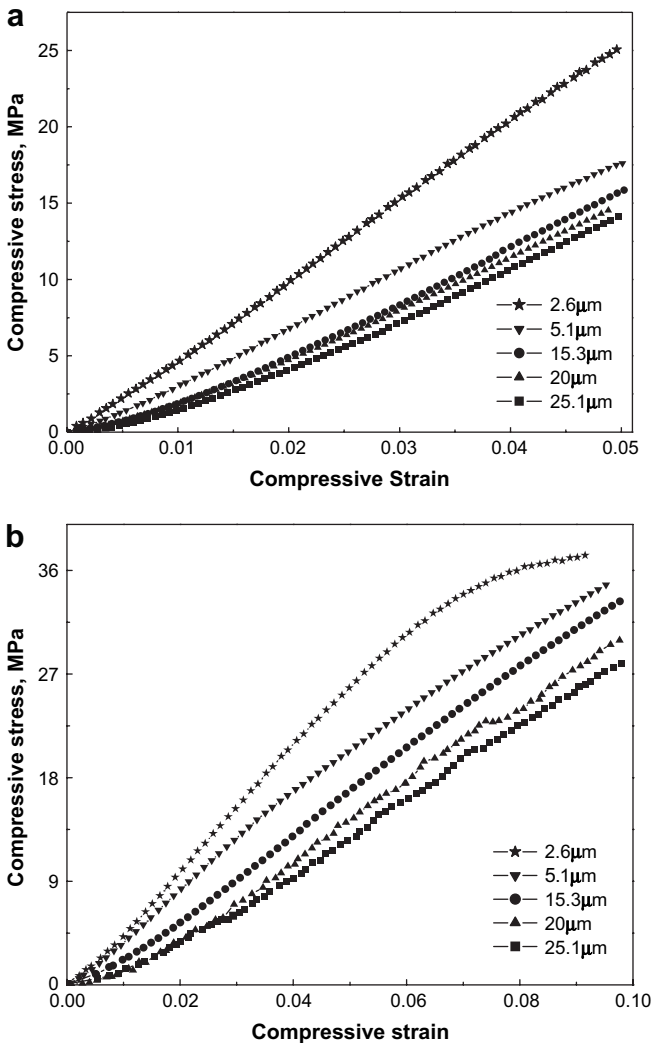

Fig. 5. Compressive stress–strain curves (a) at 5% deformation with 0.01/s strain rate and (b) at 10% deformation with 0.02/s strain rate.

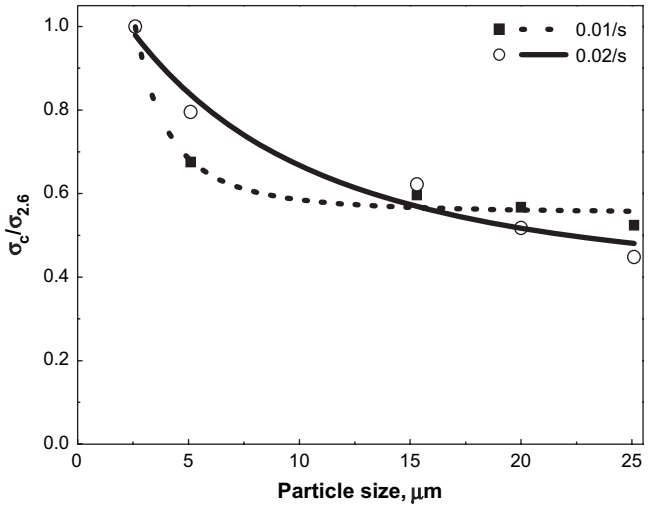

Fig. 6. Particle size dependence of the normalized stress with strain rate 0.01/s and 0.02/s at deformation level 4%.

4.1. The effect of pre-load

One of these factors is caused by the factory settings of the Hysitron TriboIndenter. During the nanoindentation, the flat punch will first contact the particle using a certain pre-load and define the corresponding height as the indentation starting contact point. The instrument keeps a defined pre-load for a certain time, and uses the acquired information to determine the thermal drift of the system. Before starting the indentation, the machine retracts a certain distance. However, the particle might not fully recover after the pre-load cycle, meaning that the indentation starts from an already deformed particle. The induced stress σ_D during the pre-load is given by:

$$\sigma_D = \frac{P_r}{\pi R^2} \tag{3}$$

Using the Hertz equation [32], the corresponding strain ε_D can be calculated as:

$$\varepsilon_D = \left(\frac{\sigma\pi}{E}\right)^{2/3} = \left(\frac{P_r}{ER^2}\right)^{2/3} \tag{4}$$

where P_r is the pre-load which was set to 1 μN for all the particles and for both standard and multi-range modes. R is the initial particle radius as shown in Fig. 2(b). E is the reduced modulus defined as $E = 4/3[(1-\nu_1^2)/E_1 + (1-\nu_2^2)/E_2]^{-1}$, in which, E_1, ν_1 and E_2, ν_2 are the elastic moduli and Poisson's ratios of the two contacted objects, respectively. The diamond is a rigid body therefore the contribution of the diamond flat punch can be regarded as negligible. The silicon substrate used in the experiment has the following characteristics, $E_{Si} = 150$ GPa [33] and $\nu_{Si} = 0.27$ [34]. For the PS–DVB particle, the elastic modulus and Poisson's ratio are both unknown, so the empirical values $E_{PS} = 1.5$ GPa and $\nu_{PS} = 0.33$ [29] are used in the analysis. With an E-modulus two order of magnitudes higher than the polymer also the contribution from the substrate can be regarded as negligible. Obviously the constant pre-load has the largest effect on the 2.6 μm diameter particle. Using the values above, the strain, ε_D, imposed onto the smallest particle during the pre-load is found to be 4.14×10^{-3} which is maximum if there is no recovery.

4.2. The adhesion effect

The contact of an elastic sphere with an undeformed flat plane is of interest since the interaction between them is applicable in problems such as post-chemical mechanical polishing cleaning [35] and the thermal and electrical conductivities between contacting rough surfaces [36] and more specifically in applications like ACA where metal-coated polymer particles are compressed between two contact pads. Two basic adhesion models have been suggested in the literature. One model developed by Johnson, Kandall and Roberts, known as JKR model [37] assumes that attractive intermolecular surface forces are confined to the area of the contact, is more suitable for large radius compliant solids. The other model by Derjaguin, Muller and Toporov, known as DMT model [38] is based on calculating the attractive forces outside of the actual contact area, and is suitable for small high modulus spheres. The improved DMT adhesion model [39] shown in Fig. 2(b) is employed to study the adhesion induced pre-strain.

According to the Lennard–Jones interaction potential [40], the attractive pressure outside the contact region $P(Z)$ is equal to:

$$P(Z) = \frac{8}{3}\frac{\Delta\gamma}{\delta}\left[\left(\frac{\delta}{Z}\right)^3 - \left(\frac{\delta}{Z}\right)^9\right] \tag{5}$$

where δ is the intermolecular distance about 0.3–0.5 nm, Z is the local separation and $\Delta\gamma$ is the energy of adhesion given by

$$\Delta\gamma = \gamma_1 + \gamma_2 - \gamma_{12} \tag{6}$$

γ_1 and γ_2 are two unattached surface energies before contact and γ_{12} is the interface energy during contact. The values of surface energy for various metals can be found in literature [40], but it is difficult to get the exact interface energy for polymer and diamond or silicon.

The adhesion force can be expressed as:

$$F_a \approx 2\pi R\Delta\gamma \tag{7}$$

Therefore the adhesion induced stress and pre-strain is calculated by:

$$\sigma_a = \frac{F_a}{\pi R^2} = \frac{2\Delta\gamma}{R} \tag{8}$$

$$\varepsilon_a = \left(\frac{\sigma\pi}{E}\right)^{2/3} = \left(\frac{2\pi\Delta\gamma}{ER}\right)^{2/3} \tag{9}$$

From the above equations it can be seen that the adhesion induced stress and strain depend on the particle size. Due to lack of values for the energy of adhesion for the present materials, the solution of the energy of adhesion is taking the empirical energy of adhesion 25 mJ/m^2 [41] as reference and arbitrary duple and quadruple values are also considered. The pre-strain is estimated using the following values for energy of adhesion: 25 mN/m, 50 mN/m and 100 mN/m. For the smallest particle, 2.6 μm in diameter, the adhesion induced pre-strain will be 1.98×10^{-3}, 3.14×10^{-3} and 5.00×10^{-3}, respectively.

Therefore, the maximum accumulative pre-stain from pre-load and adhesion is about 1% for the smallest particles. For the other four groups of particles, the accumulative pre-strain should be much smaller than that of the smallest particle. To examine the pre-strain effect, 1% accumulated pre-stain is addressed on the 25.1 μm particle. By neglecting the pre-strain of the largest particles and taking their stress–strain curves as a reference curve, the effect of pre-strain can be illustrated by translating the reference curve by the amount of pre-strain in Fig. 7. The curve marked "no pre-strain" in the reference curve is from experiment and the curve with 1% pre-strain is obtained by directly translating the "no pre-strain" curve to a new origin which is the corresponding point at 1% strain in the reference curve. It can be observed from Fig. 7 that the compressive stress–strain curve with 1% pre-strain rises only slightly compared with the stress–strain behaviour without pre-strain. It can be concluded that the effect of pre-load and adhesion on the size effect of PS–DVB particle is of secondary nature.

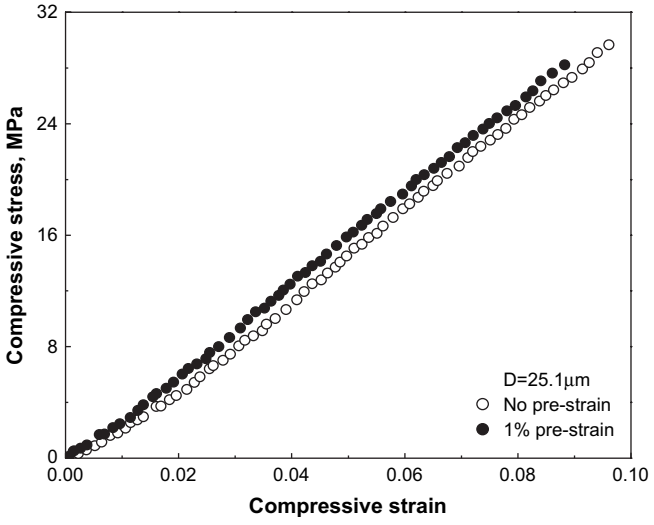

Fig. 7. The effect of estimated accumulative pre-stain 1% on the 25.1 μm diameter particles.

4.3. The surface effect

During particle preparation, polystyrene is crosslinked with divinylbenzene by an activated swelling method [42]. The degree of crosslinking modifies the microstructure of the polymer and influences the polymer properties strongly. Increasing the crosslink density can result in more heterogeneous and porous polymer [43]. The structure of a slightly crosslinked polymer seems much more homogeneous and resists larger deformation than the structure of a strongly crosslinked one. Typical techniques employed to measure crosslink degree are based on the measurement of equilibrium swelling by sedimentation in the analytical ultracentrifuge. The degree of swelling is used directly as a relative measure of the degree of crosslinking, but which do not provide spatially resolved information but rather bulk averages [44].

The average crosslink density of the tested PS–DVB particles is assessed through the measurement of the swelling degree in toluene. All five particles have the same swelling degree. The local crosslink density in PS–DVB particles is a result of the local distribution of divinylbenzene. If the crosslink distribution is not uniform in shell and core, the presence of the surface shell comes to existence. The surface shell mentioned here is different from the metal coating on the particle surface. There will be no sharp interface between the shell and the core. This surface effect might result from different hydrophilicities of the monomers involved, or due to different kinetics of the chemical reaction due to the correlation of the diffusion and crosslink reaction rate, and induce the gradient of crosslink distribution within a particle size-dependent thickness. So this crosslink distribution does influence the mechanical properties to a certain extent but it is difficult to make quantitative assessment.

Hereby the finite element analyses using ABAQUS [45] have been carried out to estimate the influence of the surface shell effect. The linear elastic material is assumed and axisymmetric elements are used to model particles. Axisymmetric analytic rigid surface is used to model the diamond flat punch. Only 5% deformation level is considered. The assigned Young's modulus E and Poisson's ratio ν for the particles are 1.5 GPa and 0.33, respectively. Different sets of shell thickness and Young's modulus are applied to get the corresponding compressive stress–strain behaviour.

The finite element solutions of the compressive stress–strain behaviours for five groups of particles at maximum 5% deformation are obtained with three sets of thickness and Young's modulus of the surface shell. The Young's modulus of particle core is kept constant 1.5 GPa. The normalized compressive stresses of five groups of particles at 4% deformation are presented in Fig. 8 from both experiment and the finite element results with 0.01/s strain rate. When the surface shell has the same elastic properties as the polymer core, namely both surface shell and polymer core have identical Young's modulus, the size effect disappeared and a horizontal line is obtained as in Fig. 8. This coincides with the viewpoint of continuum mechanics. Once the surface shell is assigned different property to the polymer core, the particles display an explicit size dependence. When the thickness and Young's modulus of the surface shell are assigned to 100 nm and 30 GPa where this Young's modulus value is totally unrealistic for polymer, the corresponding finite element solution agrees with the experiment results quite well. But this 30 GPa Young's modulus of the surface shell is obviously hypothetical. In the case of 300 nm thickness and 5.5 GPa Young's modulus of the surface shell, the modelling result

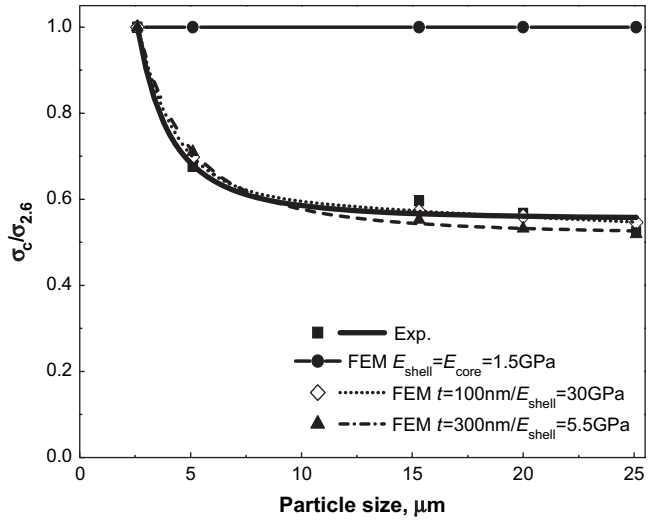

Fig. 8. Finite element solutions of the normalized compressive stress for the cases with three sets of thickness and Young's modulus of the surface shell.

would do an equally good fit with the experimental results. It should be noted that there are no experimental data available to support or disapprove the shell properties used. Nevertheless, the finite element simulation demonstrates that the hypothesis that a surface shell can play a significant role on the particle size effect is tenable.

Finally it should be mentioned that the liquid surface tension caused by absorption of water on the different surfaces has been neglected in this work. The assumption that particle is a perfect sphere after sample preparation has been made.

5. Conclusion

By using a nanoindentation-based flat punch test method, the mechanical properties of five groups of PS–DVB particles have been studied. The particles are made of same chemical compositions but different sizes, 2.6 μm, 5.1 μm, 15.3 μm, 20 μm and 25.1 μm in diameter. The nominal compressive stress–strain curves are calculated from the indentation load–displacement results. The particle stress–strain behaviour up to 5% and 10% deformation is considered. The results demonstrate that nominal stress–strain behaviour of the PS–DVB particles have significant size dependence: the smaller the size, the harder the particles.

The potential influencing factors on the mechanisms of the particle size effect are analyzed. The accumulative pre-strain induced by the presence of pre-load and the adhesion between the soft particles and the silicon substrate or the rigid flat punch seems to be of secondary nature in the size effect. The surface shell in which there is a different crosslink distribution resulting in distinct material properties from the particle core can possibly be used to explain the size effect. Further experimental investigation is necessary to verify the mechanisms of the particle size effect.

Acknowledgement

The authors acknowledge a financial support from The Research Council of Norway via a NANOMAT KMB Project.

References

[1] Oliver WC, Pharr GM. J Mater Res 1992;7:1564.
[2] Onitsch EM. Mikroskopie 1947;2:345.
[3] Manika I, Maniks J. Acta Mater 2006;54:2049.
[4] Nix WD, Gao H. J Mech Phys Solids 1998;46:411.
[5] Shu JY, Fleck NA. Int J Solids Struct 1998;35:1363.
[6] Gao H, Huang Y, Nix WD, Hutchinson JW. J Mech Phys Solids 1999;47:1239.
[7] Gerberich WW, Tymiak NI, Grunlan JC. J Appl Mech 2002;69:433.
[8] Li H, Ghosh A, Han YH. J Mater Res 1993;8:1028.
[9] Taylor GI. J Inst Metal 1938;62:307.
[10] Ugelstad J. Makromol Chem 1978;179:815.
[11] Lai Z, Liu J. IEEE Trans Compon Packag Manuf Technol Part B Adv Packag 1996;19:644.
[12] Wang X, Wang Y, Chen G, Liu J, Lai Z. IEEE Trans Compon Packag Technol 1998;21:248.
[13] Kristiansen H, Liu J. IEEE Trans Compon Packag Technol 1998;21:208.
[14] Kristiansen H, Gronlund T, Liu J. Proceeding of HDP'04; 2004. p. 259.
[15] Yim MJ, Kim HJ, Chung CK, Paik KW. Electronic components and technology conference; 2006. p. 338.
[16] Liu J, Tolvgård A, Malmodin J, Lai Z. IEEE Trans Compon Packag Technol 1999;22:186.
[17] Galloway J, Syed A, Kang W, Kim JY, Cannis J, Ka YH, et al. IEEE Trans Compon Packag Technol 2005;28:297.
[18] Dou G, Whalley D, Liu C. Proceedings of the 56th electronic components and technology conference; 2006. p. 932.
[19] Kwon WS, Paik KW. IEEE Trans Compon Packag Technol 2006;29:528.
[20] Miled K, Sab K, Roy RL. Mech Mater 2007;39:222.
[21] Cook G, Rudin A, Plumtree A. J Appl Polym Sci 1993;48:75.
[22] Dagli G, Argon AS, Cohen RE. Polymer 1995;36:2173.
[23] Alfarraj A, Nauman EB. Polymer 2004;45:8435.
[24] Jeon HK, Zhang J, Macosko CW. Polymer 2005;46:12422.
[25] Shibata M, Teramoto N, Inoue Y. Polymer 2007;48:2768.
[26] Mittal V, Matsko NB, Butte A, Morbidelli M. Polymer 2007;48:2806.
[27] Perez-Carrillo LA, Puca M, Rabelero M, Meza KE, Puig JE, Mendizabal E, et al. Polymer 2007;48:1212.
[28] VanLandingham MR, Villarrubia JS, Guthrie WF, Meyers GF. Macromol Symp 2001;167:15.
[29] Zhang ZL, Kristiansen H, Liu J. Comput Mater Sci 2007;39:305.
[30] Chow TS. J Rheol 1992;36:1707.
[31] Yang W, Ming W, Hu J, Lu X, Fu S. Colloid Polym Sci 1998;276:655.
[32] Johnson KL. Contact mechanics. 9th printing. Cambridge University Press; 2003.
[33] Available from: http://en.wikipedia.org/wiki/Silicon.
[34] Franssila S. Introduction to microfabrication. New York: John Wiley and Sons; 2004.
[35] Cooper K, Gupta A, Beaudoin. J Colloid Interface Sci 2001;234:284.
[36] Liu G, Wang QJ, Liu C. Tribol Trans 1999;42:581.
[37] Johnson KL, Kendall K, Roberts AD. Proc R Soc London Ser A 1971;324:301.
[38] Derjaguin BV, Muller VM, Toprov YP. J Colloid Interface Sci 1975;53:314.
[39] Chang WR, Etsion I, Bogy DB. ASME J Tribol 1988;110:50.
[40] Muller VM, Derjaguin BV, Toporov YP. Colloids Surf 1983;7:251.
[41] Rabinowicz E. Friction and wear of materials. 2nd ed. New York: Wiley Interscience; 1995.
[42] Ugelstad J, Berge A, Ellingsen T, Schmid R, Nilsen TN, Mork PC. Prog Polym Sci 1992;17:87.
[43] Knaebel A, Rebre SR, Lequeux F. Polym Gels Networks 1997;5:107.
[44] Sen M, Yakar A, Guven O. Polymer 1999;40:2969.
[45] Abaqus, Version 6.6, User's Manual.